Reactive Intermediates

DOI: 10.1002/anie.201409476

Influence of Ligand Architecture on Oxidation Reactions by High-Valent Nonheme Manganese Oxo Complexes Using Water as a Source of Oxygen**

Prasenjit Barman, Anil Kumar Vardhaman, Bodo Martin, Svenja J. Wörner, Chivukula V. Sastri, and Peter Comba**

Abstract: *Mononuclear nonheme Mn^{IV}=O complexes with two isomers of a bispidine ligand have been synthesized and characterized by various spectroscopies and density functional theory (DFT). The Mn^{IV}=O complexes show reactivity in oxidation reactions (hydrogen-atom abstraction and sulfoxidation). Interestingly, one of the isomers (L^1) is significantly more reactive than the other (L^2), while in the corresponding Fe^{IV}=O based oxidation reactions the L^2-based system was previously found to be more reactive than the L^1-based catalyst. This inversion of reactivities is discussed on the basis of DFT and molecular mechanics (MM) model calculations, which indicate that the order of reactivities are primarily due to a switch of reaction channels (σ versus π) and concomitant steric effects.*

High-valent manganese oxo complexes with heme and nonheme ligands have attracted much interest in the fields of bioinorganic and oxidation chemistry in the past decades. This interest is due to their importance as intermediates in the oxidation of organic substrates as well as in water oxidation by the oxygen-evolving complex (OEC) in photosystem II (PS II).[1] To reveal the chemical and physical properties of high-valent manganese oxo intermediates, a number of nonheme Mn^{IV}=O and Mn^{V}=O complexes have been reported.[2]

The ability to control the reactivity of metal oxo complexes has important consequences in a variety of chemical processes. The selective oxidation of hydrocarbon compounds and the oxidation of organic substrates by oxygen-atom transfer are fundamental transformations. One of the challenges associated with improving these processes is the choice of the ligand architecture, which helps to stabilize high-valent metal-based intermediates and optimize their reactivity.[3]

In PS II, the high-valent manganese species of the OEC uses water as a source of oxygen. In biomimetic studies, the formation of high-valent ruthenium oxo complexes has been achieved with the strong oxidants Ce^{IV} or $[Ru(bpy)_3]^{3+}$ (bpy = 2,2′-bipyridine).[4] Similarly, Fe^{IV}=O and Mn^{IV}=O complexes have also been generated using water as a source of oxygen and Ce^{IV} as a one-electron oxidant.[2a,5] Herein, we report the generation of mononuclear nonheme Mn^{IV}=O complexes with water as an oxygenation source and Ce^{IV} as a one-electron oxidant. Detailed spectroscopic and preliminary DFT studies were employed to evaluate the reactivity of the Mn^{IV}=O and the corresponding Fe^{IV}=O intermediates.

The inherently rigid adamantane-derived bispidine moiety has been used extensively as a widely variable ligand platform for transition-metal complexes, in particular also for ferryl-based oxidation catalysts,[6] and derivatives of the two isomeric pentadentate ligands L^1 (X = N, Y = CH, i.e., methylpyridine at N3) and L^2 (X = CH, Y = N, i.e., methylpyridine at N7) have been of particular interest (Figure 1).[7]

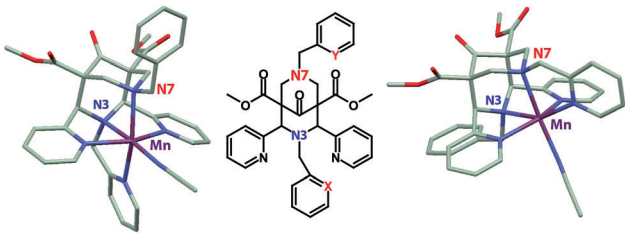

Figure 1. Plots of the X-ray structures of $[Mn^{II}(MeCN)(L^1)]$ (left (**1**), methylpyridine at N3, X = N, Y = CH, see drawing in the middle for X, Y), and $[Mn^{II}(MeCN)(L^2)]$ (right (**2**), methylpyridine at N7, X = CH, Y = N). Counterions and hydrogen atoms omitted for clarity (see the Supporting Information for further details and ORTEP plots of the two structures).

These ligands enforce square-pyramidal geometries, and the open coordination site, occupied by the oxo group in high-valent M^{n+}=O complexes, is *trans* to N3 and N7 for L^1 and L^2, respectively. This geometric variation is known to lead to striking differences in structural and electronic properties, stabilities, and reactivities, because N7 is part of a rather flexible six-membered chelate ring, while N3 is part of a very rigid five-membered chelate.[6a,8] $[Mn^{II}(L^1)(ClO_4)_2]$ (**1**) and $[Mn^{II}(L^2)(ClO_4)_2]$ (**2**) were prepared in analogy to earlier

[*] P. Barman, Dr. A. K. Vardhaman, Dr. C. V. Sastri
Department of Chemistry, Indian Institute of Technology Guwahati
Assam, 781039 (India)
E-mail: sastricv@iitg.ernet.in

Dr. B. Martin, S. J. Wörner, Prof. Dr. P. Comba
Anorganisch-Chemisches Institut and Interdisciplinary Center for Scientific Computing (IWR), Universität Heidelberg
Im Neuenheimer Feld 270, 69120 Heidelberg (Germany)
E-mail: peter.comba@aci.uni-heidelberg.de

[**] Research support was provided by the Department of Science and Technology, India (SR/S1/IC-02/2009) and the Council for Scientific & Industrial Research (01(2527)/11/EMR-II) to C.V.S. Support by the University of Heidelberg is gratefully acknowledged.

Supporting information for this article is available on the WWW under http://dx.doi.org/10.1002/anie.201409476.

reports and were structurally characterized (see the Supporting Information).[8c]

The high-valent Mn^{IV}=O intermediates, $[Mn^{IV}(O)L^1]^{2+}$ (**3**; 2 mM) and $[Mn^{IV}(O)L^2]^{2+}$ (**4**; 2 mM) were generated from their manganese(II) precursors, using cerium(IV) ammonium nitrate (CAN; 8 mM) as a one-electron oxidant in either acetonitrile/water (9:1) or acetone/water (9:1) at 278 K. The addition of CAN to the colorless solution of the manganese(II) complexes produced pale green solutions. Complex **3** exhibits an absorption spectrum with an intense band at $\lambda =$ 545 nm ($\varepsilon \approx 400\,M^{-1}cm^{-1}$) and a weak absorption in the near IR region at $\lambda = 970$ nm ($\varepsilon \approx 35\,M^{-1}cm^{-1}$). Similarly, complex **4** has electronic transitions at $\lambda = 570$ nm ($\varepsilon \approx 400\,M^{-1}cm^{-1}$) and at $\lambda = 975$ nm ($\varepsilon \approx 103\,M^{-1}cm^{-1}$; see Figure S7 in the Supporting Information). The electrospray ionization mass spectra (ESI-MS) of **3** and **4** exhibit prominent peaks with *m*/*z* 332, and the isotope patterns show that these correspond to $[Mn^{IV}(O)L^{1,2}]^{2+}$ (see Figures S8 and S9).

The reactivity of **3** and **4** was investigated with two-electron oxidation reactions such as the oxidation of the sulfur atom of thioethers. Upon addition of thioanisole to the corresponding Mn^{IV}=O species at 278 K, the intermediates decayed immediately and gave methyl phenyl sulfoxide as the major product (Figure 2a). The pseudo-first-order rate constants of the decay of **3** and **4** increased linearly with increasing thioanisole concentration, thus giving second-order rate constants, for the sulfoxidation reactions with **3** and **4** as oxidants, of $0.120(2)\,M^{-1}s^{-1}$ and $0.012(1)\,M^{-1}s^{-1}$, respectively (see Figure 2b and Table S10). Therefore, it appears that **3** reacts with thioanisole about ten times faster than the isomeric oxidant **4**. To further elucidate the reaction pathway, second-order rate constants (k_X) for the oxidation of various *para*-substituted thioanisole substrates (k_H is the second order rate constant for thioanisole; see the Supporting Information) with **4** were also determined (see Table S11 and Figure S12): a plot of the logarithm of the rate constant ratio [$\log(k_X/k_H)$] against the one-electron oxidation potentials (E^0_{OX}) of the sulfides gave a linear correlation with a slope of −10.8 (Figure 3a). Similarly large slopes were also obtained in Hammett correlations (see Figures S13 and S14). Such a large negative slope implies that the electron transfer from the sulfides to **4**, rather than a group transfer, is the rate-determining step.[9]

To further evaluate the reactivity of the two isomeric Mn^{IV}=O oxidants, H-atom abstraction reactions were also studied. The oxidation of 2,4-di-*tert*-butylphenol (2,4-$tBu_2C_6H_3OH$) with **3** and **4** yielded 2,2′-dihydroxy-3,3′,5,5′-tetra-*tert*-butylphenol. The second-order rate constants reveal that the reactivity of **3** is again larger (ca. 40 times) than that of **4** (Figure 2c and Table S10).

The O–H bond cleavage in phenols can be achieved by a H-atom abstraction or by a proton-coupled electron-transfer (PCET) mechanism.[10] PCET can be discarded when two substrates with similar O–H bond strengths and pK_a values, but with substituents with different steric demand, such as 2,6-*tert*-$Bu_2C_6H_3OH$ [BDE(O-H) = 81.65 kcal mol^{-1}; pK_a = 11.70, aqueous solution] and 2,4-*tert*-$Bu_2C_6H_3OH$ [BDE(O-H) = 81.85 kcal mol^{-1}; pK_a = 11.64, aqueous solution] show different reactivities.[10b,11] The observed approximate 50-fold rate

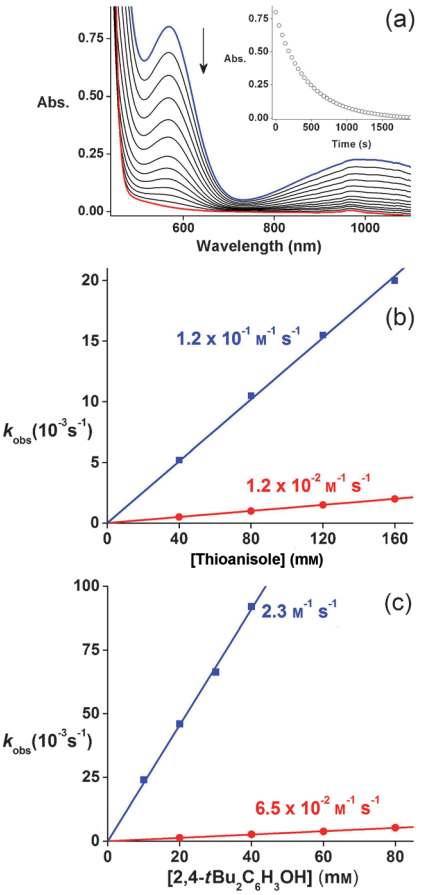

Figure 2. a) UV/Vis spectral changes of **4** (2 mM) upon addition of thioanisole (160 mM) in CH_3CN/H_2O (9:1) at 278 K (the inset shows the time trace at $\lambda = 570$ nm for the decay of Mn^{IV}=O). b) Second-order rate constants determined in the reaction of 2 mM of **3** (blue ■) and **4** (red ●) in CH_3CN/H_2O (9:1) against various concentrations of thioanisole at 278 K. c) Second order rate constants determined in the reaction of 2 mM of **3** (blue ■) and **4** (red ●) in CH_3CN/H_2O (9:1) against various concentrations of 2,4-di-*tert*-butylphenol at 233 K.

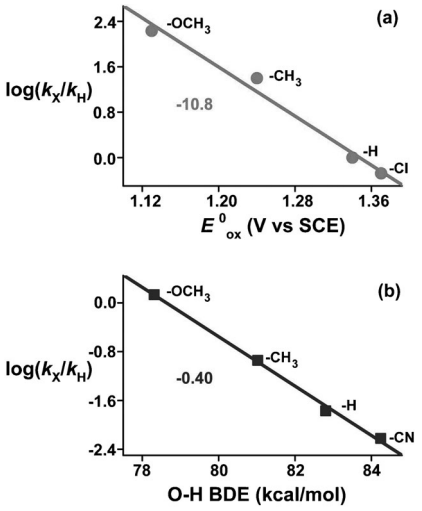

Figure 3. a) Plot of log (k_X/k_H) against E^0_{ox} values of *para*-X-thioanisoles by **4** at 278 K. b) Correlations of second-order rate constants, log (k_X/k_H), of **4** against $BDE_{O\text{-}H}$ of *p*-X-2,6-*t*$Bu_2C_6H_2OH$ at 273 K.

enhancement in the reaction of **4** with 2,4-$tBu_2C_6H_3OH$ [0.950(1) $M^{-1}s^{-1}$] as compared to 2,6-$tBu_2C_6H_3OH$, [0.017(2) $M^{-1}s^{-1}$; see Figure S16] suggests an H-atom abstraction pathway.[10,12,13]

To further substantiate the H-atom abstraction reaction with phenol, we evaluated the corresponding second-order rate constants with a series of *para*-substituted 2,6-di-*tert*-butylphenol substrates (X = OMe, Me, H, CN; see Table S17 and Figure S18). A plot of the logarithm of the rate constant ratio [$\log(k_X/k_H)$] as a function of σ_p^+ shows an excellent Hammett correlation with a ρ value of −1.6. Such a linear relationship has been used as evidence for an H-atom abstraction pathway in the oxidation of phenol O–H bonds by $[Mn^V(O)(Cz)]$ (where Cz is corrolazine), $[(L)Ru^{VI}(O)_2]^{2+}$, and $[Fe^{IV}(O)(TMC)]^{2+}$ (where TMC is tetramethyl cyclam).[10b,12,14] As further support, we have also plotted log (k_X/k_H) values against the phenol O–H bond dissociation energy (BDE), which afforded a good correlation with a slope of −0.40 (Figure 3b), thus matching well with earlier reports.[10b,12,14,15]

An interesting observation is that the corresponding iron oxidation chemistry with derivatives of L^1 and L^2 (methyl instead of benzyl groups at N7 for L^1 and N3 for L^2) follows quite a different pattern, that is, the corresponding Fe^{IV}=O complexes of L^2 are more efficient oxidants than those of L^1,[16] and this is in sharp contrast to the corresponding Mn^{IV}=O system reported here. While the substitution pattern (i.e. benzyl versus methyl) might have some influence (in a study on Cu^{II} complexes, the steric influence was studied in detail), a substantial influence is not expected since in the Fe^{IV}=O system, where the high-spin state is pseudo-Jahn–Teller active, the larger substituents should not lead to a decrease of the relative reactivity of the L^2-based ferryl complex, and the corresponding Mn^{IV}=O systems are not pseudo-Jahn–Teller active, that is, in terms of the relative reactivities, we do not expect a large effect.[17,8c] To understand the striking difference between the Fe^{IV}=O and Mn^{IV}=O systems, we have done a preliminary computational study, based on DFT (B3LYP/TZVP/Def2-TZVP[18a] and B3LYP/LANL2DZ[18b]) and force-field calculations (MOMEC force field[18c]), to analyze the steric and electronic factors which determine the reactivity (C–H activation with cyclohexane as substrate, using the methyl-substituted ligands; see the Supporting Information for details). We have optimized the metal oxo starting structures, the preequilibrium of the reactants with the substrate, the transition states for C–H abstraction, and the emerging intermediates (M^{III}–OH, for M = Mn, Fe, both isomers (L^1, L^2) and all relevant spin states).

For the iron-based oxidants, the ferryl complexes are all in the $S = 1$ intermediate spin state (stabilized by approx. 20 kJ mol^{-1} with respect to the $S = 2$ state), and the reaction crosses to the $S = 2$ high-spin surface in the H abstraction step, that is, the transition state has an $S = 2$ configuration (stabilized by approx. 50 kJ mol^{-1}; see Table S27). For the manganese-based system, the ground state of Mn^{IV}=O for both isomers is $S = 3/2$ (stabilized by approx. 25 kJ mol^{-1}) and the transition state is low-spin, that is, $S = 1/2$ (stabilized by approx. 20 kJ mol^{-1}; see Table S27). For the $S = 2$ ferryl species, the electrophilic attack may proceed through two different pathways: 1) the σ pathway [linear M-O-H(substrate) orientation] involving the iron d_{z^2} orbital, and 2) the π pathway [bent M-O-H(substrate) orientation] involving a d_π orbital (d_{xz}, d_{yz}).[19] In contrast, for the d^3 Mn^{IV}=O system, specifically in its $S = 1/2$ electronic configuration, the π pathway is favored. As therefore expected, all relevant optimized iron-based transition states are linear, and those of the manganese-based system are bent (M-O-H angles of approx. 175° vs. 130°; see Figure 4 and Table S29).[20]

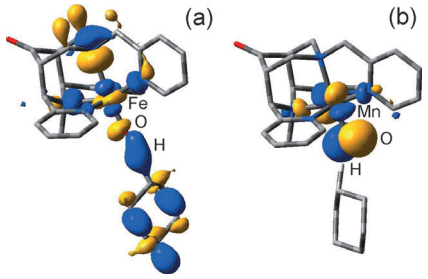

Figure 4. Orbital plots of the H abstraction intermediates: a) $Fe^{IV}(O)(L^2)]^{2+}$ (αSOMO−1); b) $Mn^{IV}(O)(L^2)]^{2+}$ (αSOMO); isovalues = 0.04.

The computed spin densities suggest that the ferryl oxidants in their $S = 1$ ground state have about equal spin density on the Fe and O centers. In Mn^{IV}=O ($S = 3/2$) most of the unpaired electron density is on the metal center (see Table S29). In the transition states most of the spin density is on the $S = 2$ Fe and on the $S = 1/2$ Mn centers (Figure 4). That is, the ferryl system in its ground state is further on its way towards an Fe^{III}-oxyl-radical description than the manganese system and, in both cases, partial electron transfer is well on its way.

Both isomers are very similar in their behavior with both metal ions. The computed energy barriers for the rate-determining H-abstraction steps are in very good agreement with the experimental data for the iron-based system, but less clear cut for the manganese-based system (Fe-L^2: 33 kJ mol^{-1}, Fe-L^1: 44 kJ mol^{-1}; Mn-L^1: 71 kJ mol^{-1}, Mn-L^2: 65 kJ mol^{-1}; Table S27): while DFT predicts the correct order of reactivities for Fe^{IV}=O by 11 kJ mol^{-1}, the two isomers are (within the error limit) identical for the Mn^{IV}=O oxidants (energy difference of 6 kJ mol^{-1}). While this is not satisfactory, one needs to appreciate that the error limit for the iron systems, with the theoretical setup used, is on the order of 10 kJ mol^{-1}. For Mn^{IV}=O, where less thorough bench marking is available, the results therefore are within the error limit also in agreement with the experimental data.[21,22] Importantly, there is a constant shift of relative energies, approximately 2–3 kJ mol^{-1}, between the two basis sets used. That is, the activation barriers of the two isomers are approximately identical and largely independent of the basis set. The main result from the DFT analysis is, therefore, that the two systems (Fe^{IV}=O versus Mn^{IV}=O) follow two different reaction channels (σ versus π) and that the relative activation barriers of the σ channel for the pair of Fe^{IV}=O isomers are accurately predicted, while those for the pair of Mn^{IV}=O isomers following the π channel are not.

From the transition-state structures (linear versus bent; see Figure 4 for two examples) it emerges that steric strain might be a decisive factor for the energy of the four transition-state structures (L^1, L^2, linear and bent). We therefore have performed the four corresponding force-field calculations along the torsional rotation around the M=O bond (van-der-Waals energy as a function of the torsional angle, rigid geometry of the L^nM-O-H substructure, fully refined substrate and substrate orientation at each point of the torsional coordinate; see Figure 5 and the Supporting Information for details). It emerges that the lowest energy orientations are those found in the DFT optimizations, thus suggesting that steric strain is of importance for the choice of the pathway. Importantly, for the linear structure, there is basically free rotation of the cyclohexyl substrate around the M=O axis, and both isomers (L^1 and L^2) are, in terms of steric energy, degenerate. That is, in the case of the iron-based systems, where both isomers react along the σ pathway, there are electronic reasons for the enhanced reactivity of the L^2-based system. Interestingly, the reactivities of the iron-based complexes have been experimentally shown to be correlated with the $Fe^{IV/III}$ redox potential, and this then suggests that the reactivities are correlated to the driving force of the electron-transfer step.[3c]

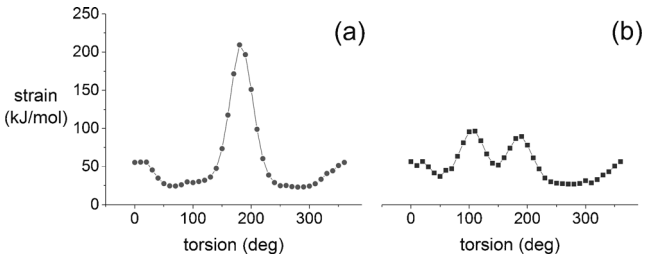

Figure 5. Plot of the van der Waals energies of the transition-state structures (Mn complexes, rotation of the cyclohexyl substrate around the Mn–O bond, for details see Supporting Information). a) L^2-based complex. b) L^1-based complex.

For the manganese-based bent system, the minimum-energy transition-state structures are the lowest energy minima on the steric energy surface, but for the L^1-based system the barrier is significantly smaller and there is also another minimum, which is less than 10 kJ mol^{-1} higher in energy (Figure 5). The minimum steric strain imposed by the L^2-based system is approximately 4 kJ mol^{-1} lower, that is, in good agreement with the DFT results, and thus suggests that most of the energetic difference between the two isomeric transition states is steric in nature (see Table S19 and Figure S20). We have also done preliminary force-field calculations with the phenyl substituents in L^1 and L^2, which show that steric effects are significantly larger for the L^2-based system, and this is in agreement with the experimental data reported here.

The most important observation emerging from the force-field calculations visualized in Figure 5 is that the molecular surface of the L^1-based system is significantly more open for a π attack than that of the L^2-based complex, and this is expected: the N3 and N7 methyl (or phenyl) substituents are a major reason for blocking the approach of the substrate, and it is a known and well-understood feature of bispidine coordination geometry that the metal–N7 bonds are generally more flexible and longer than the metal–N3 bonds.[6] We suggest that this is the reason for the observations emerging from Figure 5 and the strikingly different activation barriers for the π pathway of the manganese-based systems. Clearly, what emerges is an entropy effect, which is not captured by the DFT analysis presented here. A quantitative analysis of this effect would require an (ab initio) molecular dynamics analysis, which is outside the scope of this study.

The important DFT-based prediction is that the Fe^{IV}=O systems react through the σ pathway and the Mn^{IV}=O complexes through the π channel. Therefore, for the sterically less demanding iron-based oxidations, the DFT-predicted relative activation barriers are accurate. For the manganese-based system, the situation is more complex: the DFT-based and the MM-based steric analysis are in good agreement and predict similar activation barriers for the two isomers. However, the MM analysis also suggests that the approach of the substrate is, as predicted from extensive structural work of bispidine complexes, favored for the L^1-based system.[6] The main point emerging from the current report is that between the manganese and iron systems, there are drastic changes in subtle mechanistic features, which are responsible for the switch in reactivity between the two isomers based on L^1 and L^2: while the iron systems may evade steric strain through the σ pathway, the manganese systems do not have this possibility and react through the π pathway, that is, the sterically demanding bent structures. While these pathways have been appreciated before, they have rarely been used to interpret subtle differences in reactivities as observed here. It appears that other striking and so far not satisfactorily explained reactivity differences might find similar interpretations.[3c]

Received: September 25, 2014
Revised: November 17, 2014
Published online: December 29, 2014

Keywords: density functional calculations · isomers · manganese · oxidation · structure elucidation

[1] a) S. Tanase, E. Bouwman, *Advances in Inorganic Chemistry*, *Vol. 58* (Eds.: R. van Eldik, J. Reedijk), Elsevier, San Diego, **2006**, pp. 29–75; b) I. Garcia-Bosch, A. Company, C. W. Cady, S. Styring, W. R. Browne, X. Ribas, M. Costas, *Angew. Chem. Int. Ed.* **2011**, *50*, 5648–5653; *Angew. Chem.* **2011**, *123*, 5766–5771.

[2] a) S. C. Sawant, X. Wu, J. Cho, K.-B. Cho, S. H. Kim, M. S. Seo, Y.-M. Lee, M. Kubo, T. Ogura, S. Shaik, W. Nam, *Angew. Chem. Int. Ed.* **2010**, *49*, 8190–8194; *Angew. Chem.* **2010**, *122*, 8366–8370; b) W. Liu, X. Huang, M.-J. Cheng, R. J. Nielsen, W. A. Goddard III, J. T. Groves, *Science* **2012**, *337*, 1322–1325; c) T. Taguchi, R. Gupta, B. Lassalle-Kaiser, D. W. Boyce, V. K. Yachandra, W. B. Tolman, J. Yano, M. Hendrich, A. S. Borovik, *J. Am. Chem. Soc.* **2012**, *134*, 1996–1999; d) D. F. Leto, R. Ingram, V. W. Day, T. A. Jackson, *Chem. Commun.* **2013**, *49*, 5378–5380; e) H. M. Neu, T. Yang, R. A. Baglia, T. H. Yosca, M. T. Green, M. G. Quesne, S. P. de Visser, D. P. Goldberg, *J.*

Am. Chem. Soc. **2014**, *136*, 13845 – 13852; f) J. Chen, Y.-M. Lee, K. M. Davis, X. Wu, M. S. Seo, K.-B. Cho, H. Yoon, Y. J. Park, S. Fukuzumi, Y. N. Pushkar, W. Nam, *J. Am. Chem. Soc.* **2013**, *135*, 6388 – 6391; g) S. D. Hicks, D. Kim, S. Xiong, G. A. Medvedev, J. Caruthers, S. Hong, W. Nam, M. M. Abu-Omar, *J. Am. Chem. Soc.* **2014**, *136*, 3680 – 3686.

[3] a) M. Costas, L. Que, Jr., *Angew. Chem. Int. Ed.* **2002**, *41*, 2179 – 2181; *Angew. Chem.* **2002**, *114*, 2283 – 2285; b) S. Hong, Y.-M. Lee, K.-B. Cho, K. Sundaravel, J. Cho, M. J. Kim, W. Shin, W. Nam, *J. Am. Chem. Soc.* **2011**, *133*, 11876 – 11879; c) D. Wang, K. Ray, M. J. Collins, E. R. Farquhar, J. R. Frisch, L. Gömez, T. A. Jackson, M. Kerscher, A. Waleska, P. Comba, M. Costas, L. Que, Jr., *Chem. Sci.* **2013**, *4*, 282 – 291.

[4] a) S. Romain, L. Vigara, A. Llobet, *Acc. Chem. Res.* **2009**, *42*, 1944 – 1953; b) C.-M. Che, V. W.-W. Yam, T. C. W. Mak, *J. Am. Chem. Soc.* **1990**, *112*, 2284 – 2291; c) Y. Hirai, T. Kojima, Y. Mizutani, Y. Shiota, K. Yoshizawa, S. Fukuzumi, *Angew. Chem. Int. Ed.* **2008**, *47*, 5772 – 5776; *Angew. Chem.* **2008**, *120*, 5856 – 5860; d) A. Sartorel, M. Carraro, G. Scorrano, R. De Zorzi, S. Geremia, N. D. McDaniel, S. Bernhard, M. Bonchio, *J. Am. Chem. Soc.* **2008**, *130*, 5006 – 5007; e) Y. V. Geletii, B. Botar, P. Kgerler, D. A. Hillesheim, D. G. Musaev, C. L. Hill, *Angew. Chem. Int. Ed.* **2008**, *47*, 3896 – 3899; *Angew. Chem.* **2008**, *120*, 3960 – 3963.

[5] a) Y.-M. Lee, S. N. Dhuri, S. C. Sawant, J. Cho, M. Kubo, T. Ogura, S. Fukuzumi, W. Nam, *Angew. Chem. Int. Ed.* **2009**, *48*, 1803 – 1806; *Angew. Chem.* **2009**, *121*, 1835 – 1838.

[6] a) P. Comba, M. Kerscher, W. Schiek, *Prog. Inorg. Chem.* **2007**, *55*, 613 – 704; b) P. Comba in *Molecular Catalysis* (Eds.: L. H. Gade, P. Hofmann), Wiley-VCH, Weinheim, **2014**, pp. 123 – 145.

[7] M. Bukowski, P. Comba, C. Limberg, M. Merz, L. Que, Jr., T. Wistuba, *Angew. Chem. Int. Ed.* **2004**, *43*, 1283 – 1287; *Angew. Chem.* **2004**, *116*, 1303 – 1307.

[8] a) P. Comba, A. Lienke, *Inorg. Chem.* **2001**, *40*, 5206 – 5209; b) A. E. Anastasi, P. Comba, J. McGrady, A. Lienke, H. Rohwer, *Inorg. Chem.* **2007**, *46*, 6420 – 6426; c) P. Comba, B. Kanellakopulos, C. Katsichtis, A. Lienke, H. Pritzkow, F. Rominger, *J. Chem. Soc. Dalton Trans.* **1998**, 3997 – 4001.

[9] a) Y. Goto, T. Matsui, S.-I. Ozaki, Y. Watanabe, S. Fukuzumi, *J. Am. Chem. Soc.* **1999**, *121*, 9497 – 9502; b) J. Park, Y. Morimoto, Y.-M. Lee, W. Nam, S. Fukuzumi, *J. Am. Chem. Soc.* **2011**, *133*, 5236 – 5239; c) P. Comba, S. Fukuzumi, H. Kotani, S. Wunderlich, *Angew. Chem. Int. Ed.* **2010**, *49*, 2622 – 2625; *Angew. Chem.* **2010**, *122*, 2679 – 2682; d) A. K. Vardhaman, P. Barman, S. Kumar, C. V. Sastri, D. Kumar, S. P. de Visser, *Angew. Chem. Int. Ed.* **2013**, *52*, 12288 – 12292; *Angew. Chem.* **2013**, *125*, 12514 – 12518.

[10] a) I. J. Rhile, J. M. Mayer, *J. Am. Chem. Soc.* **2004**, *126*, 12718 – 12719; b) D. T. Y. Yiu, M. F. W. Lee, W. W. Y. Lam, T.-C. Lau, *Inorg. Chem.* **2003**, *42*, 1225 – 1232.

[11] A. Habibi-Yangjeh, M. Danandeh-Jenagharad, M. Nooshyar, *J. Mol. Model.* **2006**, *12*, 338 – 347.

[12] D. E. Lansky, D. P. Goldberg, *Inorg. Chem.* **2006**, *45*, 5119 – 5125.

[13] M. Lucarini, P. Pedrielli, G. F. Pedulli, S. Cabiddu, C. Fattuoni, *J. Org. Chem.* **1996**, *61*, 9259 – 9263.

[14] C. V. Sastri, L. Lee, K. Oh, Y. J. Lee, J. Lee, T. A. Jackson, K. Ray, H. Hirao, W. Shin, J. A. Halfen, J. Kim, L. Que, Jr., S. Shaik, W. Nam, *Proc. Natl. Acad. Sci. USA* **2007**, *104*, 19181 – 19186.

[15] P. Mulder, O. W. Saastad, D. Griller, *J. Am. Chem. Soc.* **1988**, *110*, 4090 – 4092.

[16] a) M. R. Bukowski, P. Comba, A. Lienke, C. Limberg, C. Lopez de Laorden, R. Mas-Ballesté, M. Merz, L. Que, Jr., *Angew. Chem. Int. Ed.* **2006**, *45*, 3446 – 3449; *Angew. Chem.* **2006**, *118*, 3524 – 3528; b) J. Madhavan, P. Comba, M. Maurer, P. Vadivelu, V. Venuvanalingham, *Dalton Trans.* **2011**, *40*, 11276 – 11281; c) P. Comba, M. Maurer, P. Vadivelu, *Inorg. Chem.* **2009**, *48*, 10389 – 10396.

[17] A. Bentz, P. Comba, R. J. Deeth, M. Kerscher, B. Seibold, H. Wadepohl, *Inorg. Chem.* **2008**, *47*, 9518 – 9527.

[18] a) A. Schaefer, C. Huber, R. Ahlrichs, *J. Chem. Phys.* **1994**, *100*, 5829 – 5835; F. Weigend, *Phys. Chem. Chem. Phys.* **2006**, *8*, 1057 – 1065; b) P. J. Hay, W. R. Wadt, *J. Chem. Phys.* **1985**, *82*, 299 – 310; c) J. E. Bol, C. Buning, P. Comba, J. Reedijk, M. Ströhle, *J. Comput. Chem.* **1998**, *19*, 512 – 523.

[19] a) E. I. Solomon, S. D. Wong, L. V. Liu, A. Decker, M. S. Chow, *Curr. Opin. Chem. Biol.* **2010**, *13*, 99 – 113; b) S. Ye, F. Neese, *Proc. Natl. Acad. Sci. USA* **2011**, *108*, 1228 – 1233; c) C. Geng, S. Ye, F. Neese, *Angew. Chem. Int. Ed.* **2010**, *49*, 5717 – 5720; *Angew. Chem.* **2010**, *122*, 5853 – 5856; d) S. Ye, C.-Y. Geng, S. Shaik, F. Neese, *Phys. Chem. Chem. Phys.* **2013**, *15*, 8017 – 8030; e) M. Srnec, S. D. Wong, E. I. Solomon, *Dalton Trans.* **2014**, *43*, 17567 – 17577.

[20] We have not completed a computational analysis for the sulfoxidation reaction. From published work on the iron-based systems it emerges, however, that depending on the isomer (oxo group *trans* to either N3 or N7), the lowest energy transition state ($S = 2$) has either linear or bent structures,[16b] thus suggesting that in the iron system, there might be changes in structure and concomitantly in reactivity resulting from subtle changes in the steric demand of the substrate.

[21] S. P. de Visser, M. G. Quesne, B. Martin, P. Comba, U. Ryde, *Chem. Commun.* **2014**, *50*, 412 – 414.

[22] K.-B. Cho, S. Shaik, W. Nam, *J. Phys. Chem. Lett.* **2012**, *3*, 2851 – 2856.

